SCIENCE CHINA
Information Sciences

• Supplementary File •

High Linearity GaN HEMT by Optimized Three-Dimensional-Gated Modulation via Top-MIS-Gate Nanowire Channel Structure

Can GONG[1], Minhan MI[1*], Yuwei ZHOU[1], Pengfei WANG[1], Hanzhen Li[1], Xinyi WEN[1], Ting MENG[1], Sirui AN[1], Xiang DU[1], Kai CHENG[2], Meng ZHANG[1], Qing ZHU[1], Xiaohua MA[1] & Yue HAO[1]

[1]*State Key Discipline Laboratory of Wide Band Gap Semiconductor Technology, Xidian University, Xi'an 710071, China;*
[2]*Enkris Semiconductor Inc., Suzhou 215123, China*

Appendix A Device Fabrication

The epi-layers of heterojunction were grown by metal-organic-chemical vapor deposition (MOCVD) on SiC substrate, which comprise a 20 nm in-situ SiN cap layer, a 6 nm $Al_{0.25}GaN$ barrier layer, and GaN buffer layer. Because the stress-strain from in-situ SiN cap induces enhanced piezoelectric polarization of the barrier, the two-dimensional electron gas (2DEG) density and mobility were measured as 1.02×10^{13} cm^{-2} and 2102 cm^2/V·s by the room temperature Hall measurement.

For the purpose of comparison, planar-HEMT, NC-HEMT, MIS-planar-HEMT, and TMGNC-HEMT were fabricated on the same wafer. The four kinds of the HEMTs' fabrication process started with the definition of the ohmic contact region. And the in-situ SiN on the ohmic contact region was etched by CF_4-based plasma. Then, the Ti/Al/Ni/Au ohmic metals were evaporated, followed by rapid thermal annealing at 860 ℃ for 60 s in N_2 atmosphere. After that, the device isolation was achieved by ion implantation. Until this point, the fabrication process was the same for planar-HEMT, NC-HEMT, and TMGNC-HEMT. Therefore, the four kinds of the HEMTs have the same source-drain distance (L_{SD}) of 1.5 μm.

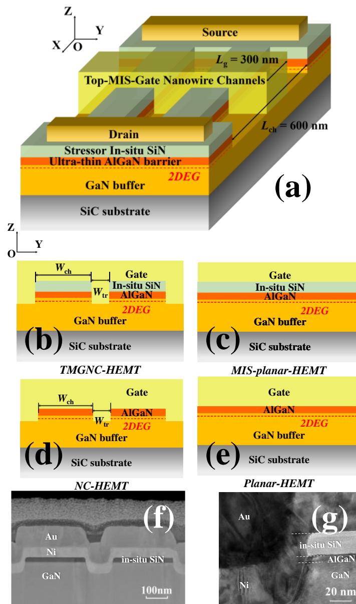

Figure A1 (a) Schematic diagram of TMGNC-HEMT. (b)-(e) The cross-section diagrams of TMGNC-HEMT, MIS-planar-HEMT, NC-HEMT, and Planar-HEMT, respectively. (f) SEM image of the TMGNC structure. (g) HRTEM image of one side of the TMGNC structure.

* Corresponding author (email: miminhan@qq.com)

The schematic diagram of the TMGNC-HEMT is shown in Fig.A1(a). For TMGNC-HEMT, after device isolation, the nanowire channel patterns were defined by electron beam lithography (EBL), and followed by a CF_4-based plasma etching and a BCl_3/Cl_2-based plasma etching were used to form periodic trenches. As shown in Fig.A1(f), the Top-MIS-Gate nanowire channel width ($W_{\rm ch}$) is about 300 nm and the trench width ($W_{\rm tr}$) is about 100 nm. Finally, the Ni/Au gate metals were deposited by electron beam evaporation. The gate length ($L_{\rm g}$) was 300 nm. And the HRTEM image of TMGNC structure was shown in Fig.A1(g). For MIS-planar-HEMT, the same $L_{\rm g}$ of 300 nm was defined by EBL after isolation and followed by the deposition of Ni/Au gate metals. But for planar-HEMT, following by device isolation, the same $L_{\rm g}$ was defined by EBL and the in-situ SiN cap under the gate was etched by CF_4-based plasma to ensure available ON/OFF capability. Then the Ni/Au gate metals were deposited. For NC-HEMT, the same dimension of nanowire channel structure (($W_{\rm ch}$/($W_{\rm tr}$) was fabricated as TMGNC-HEMT. However, after EBL defining the same length of gate region, the in-situ SiN cap under the gate was etched by CF_4-based plasma. Afterwards, the Ni/Au gate metals were evaporated. Therefore, compared with TMGNC-HEMT, there was no in-situ SiN under its top gate for NC-HEMT with the same $L_{\rm g}$. The cross-section diagrams of the four kinds of HEMTs under the gate (Y-O-Z plane, along the gate width direction) are shown in Fig.A1(b)-(e). Eventually, the four kinds of HEMTs have the same total gate width of 2×50 µm. Note that the current and transconductance of the three HEMTs in this work are normalized using the total actual gate width rather than the effective gate width.

Appendix B Discussion on gate control of MIS-planar-HEMT and TMGNC-HEMT

In terms of device structure, the channel is controlled longitudinally by Top-MIS gate only for MIS-planar-HEMT. However, for TMGNC-HEMT, lateral sidewall gate control of the channel is added. By the simulation in Fig.B2, the channel cannot be controlled effectively by only the Top-MIS gate. Therefore, the channel of TMGNC-HEMT is mainly controlled by the sidewall gate. And for the Top-MIS-gate nanowire channel structure, this is a gradual lateral control, as shown in Fig.B3.

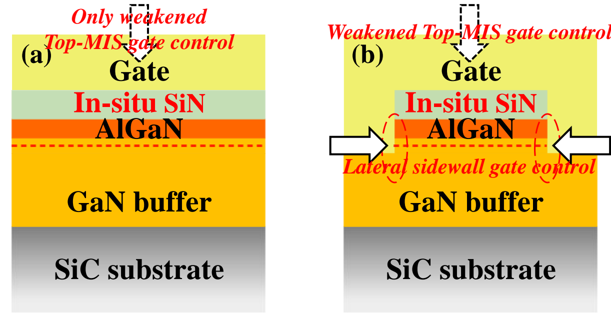

Figure B1 The differences of (a) MIS-planar-HEMT and (b) TMGNC-HEMT in terms of device structure and gate-control dimensions.

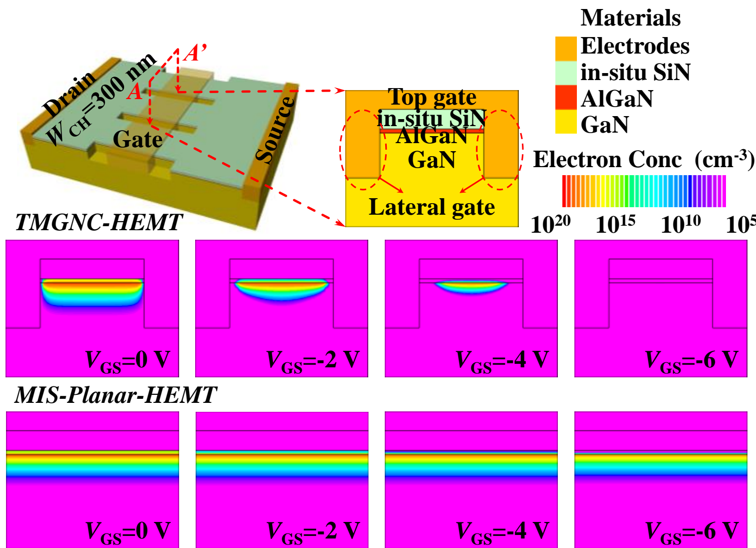

Figure B2 Simulation on the variation of electron concentration distribution of a TMGNC-HEMT and a MIS-planar-HEMT with 20 nm SiN. The electron concentration varying with $V_{\rm GS}$ decreasing from 0 to -6 V.

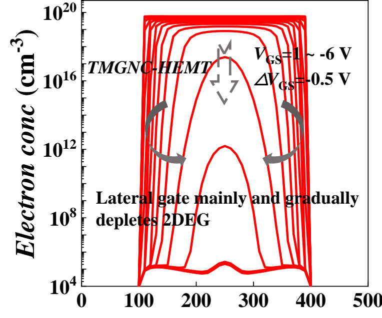

Figure B3 The electron concentration varying with V_{GS} decreasing from 1 to -6 V of TMGNC-HEMT. Gradual lateral depletion effect contributes to the improvement of G_{m} flatness.

The simulation results are reflected in the transfer characteristics. Because the 2DEG channel of the MIS-planar-HEMT cannot be completely pitched off with decreasing V_{GS}, as shown in Fig.B2. Therefore, as shown in Fig.B4, the MIS-planar-HEMT has a poor off-state current density of transfer characteristic.

Besides, due to the absence of the gradual lateral control by the sidewall gate, the G_{m} is not flat at V_{DS} of 18 V as shown in Fig.B5 (a). Therefore, TMGNC-HEMT, which inhibits top-gate depletion while ensuring gradual sidewall gate depletion, has obvious linear advantages as shown in Fig.B5 (b).

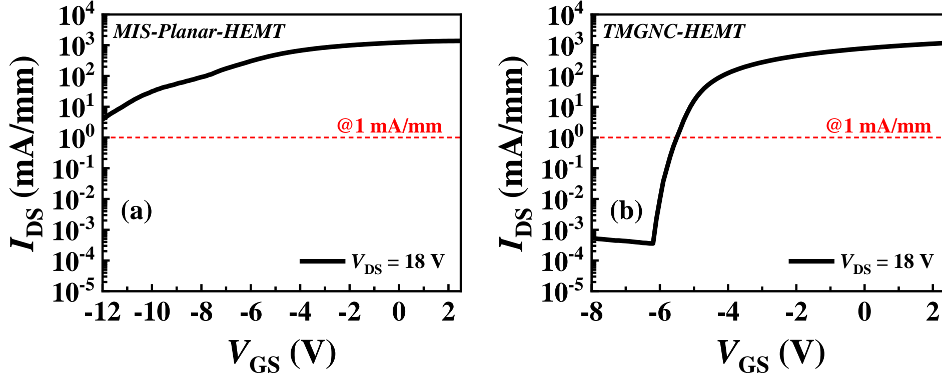

Figure B4 (a) Transfer characteristics of the MIS-planar-HEMT and (b) the TMGNC-HEMT in log coordinate.

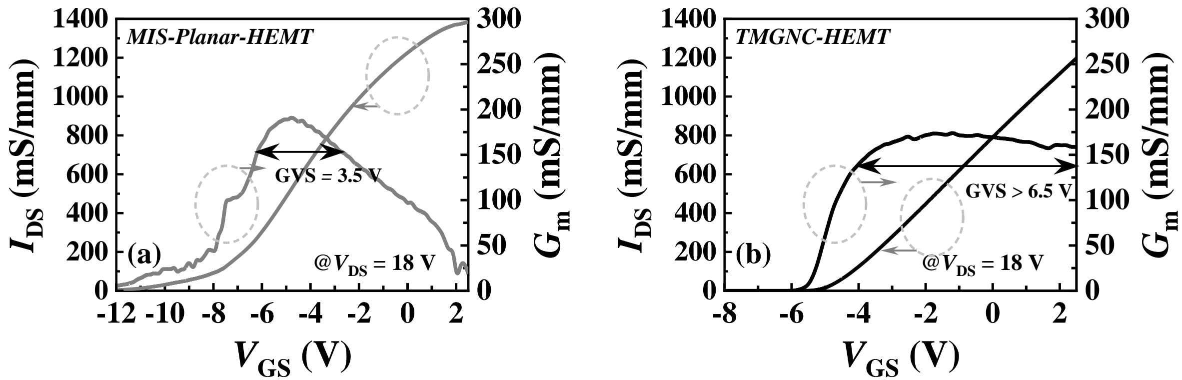

Figure B5 (a) The I_{DS}-V_{GS} and G_{m}-V_{GS} characteristics of the MIS-planar-HEMT and (b) the TMGNC-HEMT.

Appendix C High-Resolution Figure 1

For the convenience of editors and reviewers reviewing this manuscript, Figure 1 in high resolution is listed in Appendix C.

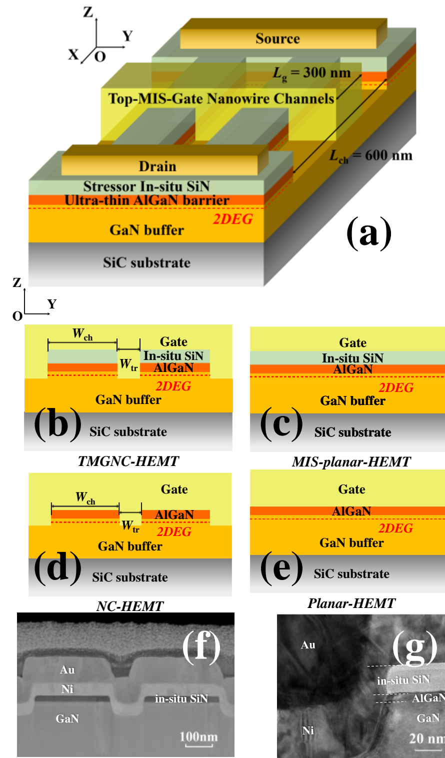

Figure C1 (color online) (a) Schematic diagram of TMGNC-HEMT. (b)-(e) The cross-section diagrams of TMGNC-HEMT, MIS-planar-HEMT, NC-HEMT, and Planar-HEMT, respectively. (f) SEM image of the TMGNC structure. (g) HRTEM image of one side of the TMGNC structure.

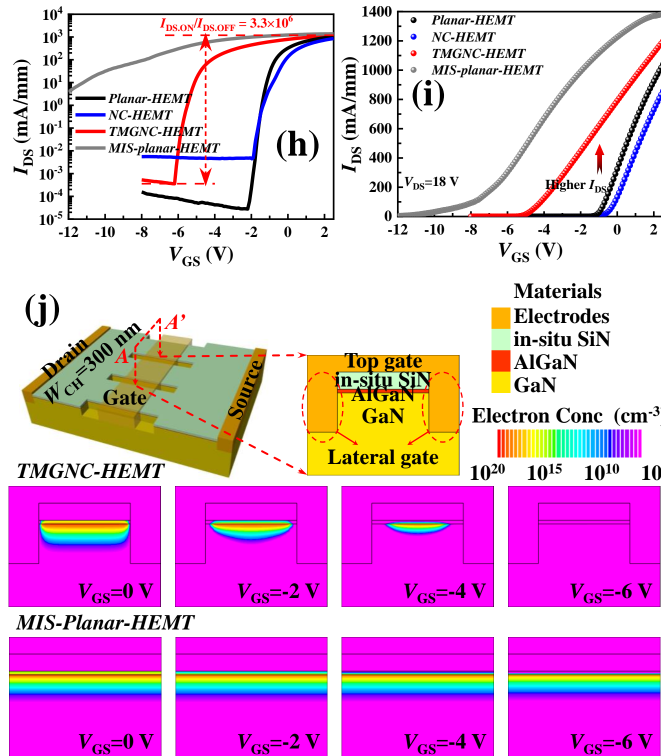

Figure C2 (color online) Comparison of $I_{\rm DS}$-$V_{\rm GS}$ characteristics in log coordinate (h) and in linear coordinate (i) of the four kinds of HEMTs at $V_{\rm DS}$ of 18 V. (j) Simulation on the variation of electron concentration distribution for the TMGNC-HEMT and planar-HEMT with in-situ SiN under the gate (MIS-planar-HEMT) when $V_{\rm GS}$ drops from 0 to -6 V.

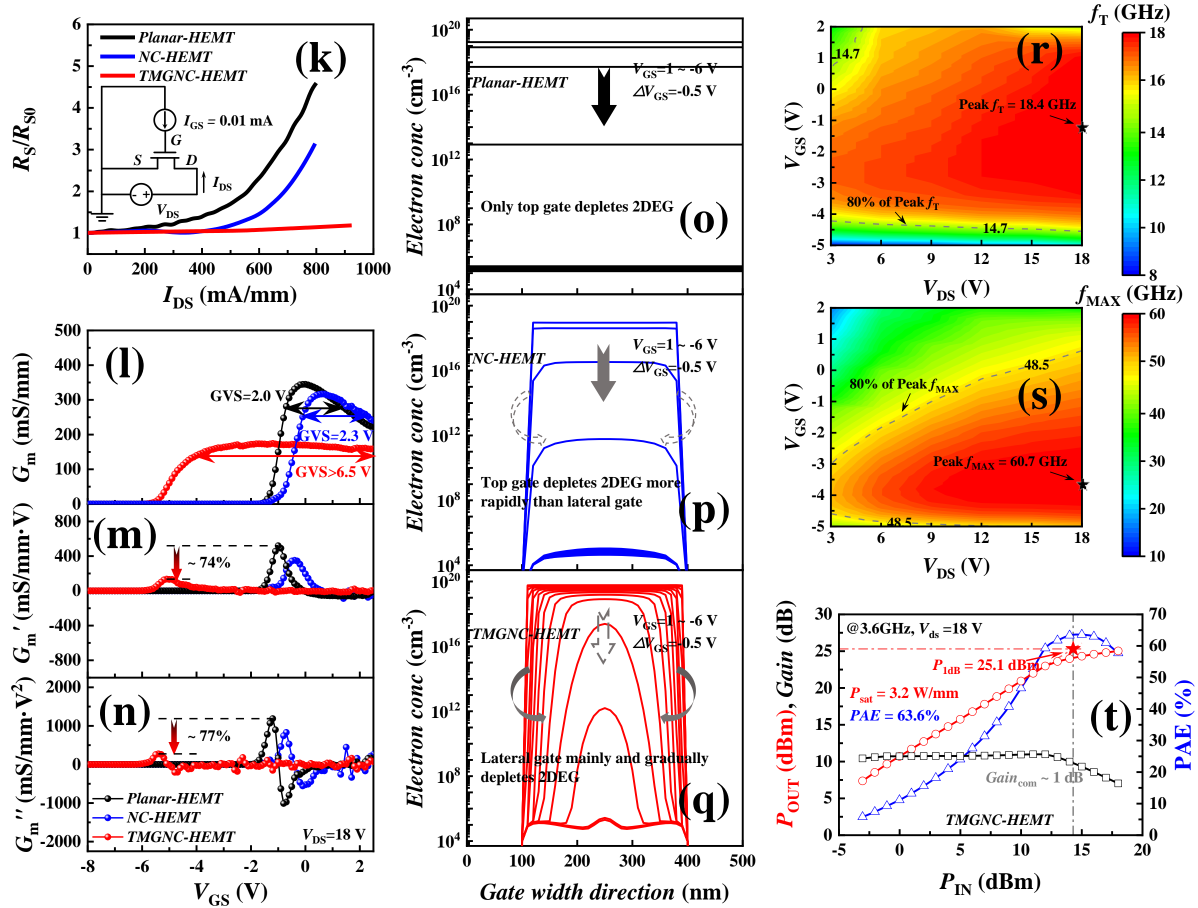

Figure C3 (color online) (k) Normalized source access resistance (R_S/R_{S0}) of planar-HEMT, NC-HEMT, and TMGNC-HEMT with increasing I_{DS}. Comparison of G_m (l), the first derivative (m), and the second derivative (n) of G_m characteristics of the planar-HEMT, NC-HEMT, and TMGNC-HEMT. The electron concentration varying with V_{GS} decreasing from 1 to -6 V of (o) planar-HEMT, (p) NC-HEMT, and (q) TMGNC-HEMT at the 2DEG channel position along the gate width direction. Gradual lateral depletion effect of TMGNC-HEMT contributes to the improvement of G_m flatness. The variations in (r) f_T and (s) f_{MAX} as a function of the gate and drain voltages of TMGNC-HEMT. The peak f_T and the peak f_{MAX} are 18.4 GHz and 60.7 GHz, respectively. (t) Load-pull measurement at V_{DS} of 18 V for TMGNC-HEMT at 3.6 GHz.